nature biotechnology

LETTERS

https://doi.org/10.1038/s41587-020-0495-2

Check for updates

Morphing electronics enable neuromodulation in growing tissue

Yuxin Liu[1,8], Jinxing Li[2,8], Shang Song[3,8], Jiheong Kang[2,7], Yuchi Tsao[4], Shucheng Chen[2], Vittorio Mottini[2], Kelly McConnell[3], Wenhui Xu[5], Yu-Qing Zheng[2], Jeffrey B.-H. Tok[2], Paul M. George[3,6,9] ✉ and Zhenan Bao[2,9] ✉

Bioelectronics for modulating the nervous system have shown promise in treating neurological diseases[1–3]. However, their fixed dimensions cannot accommodate rapid tissue growth[4,5] and may impair development[6]. For infants, children and adolescents, once implanted devices are outgrown, additional surgeries are often needed for device replacement, leading to repeated interventions and complications[6–8]. Here, we address this limitation with morphing electronics, which adapt to in vivo nerve tissue growth with minimal mechanical constraint. We design and fabricate multilayered morphing electronics, consisting of viscoplastic electrodes and a strain sensor that eliminate the stress at the interface between the electronics and growing tissue. The ability of morphing electronics to self-heal during implantation surgery allows a reconfigurable and seamless neural interface. During the fastest growth period in rats, morphing electronics caused minimal damage to the rat nerve, which grows 2.4-fold in diameter, and allowed chronic electrical stimulation and monitoring for 2 months without disruption of functional behavior. Morphing electronics offers a path toward growth-adaptive pediatric electronic medicine.

Although bioelectronic devices, such as the vagus nerve stimulator and deep brain stimulator, are being actively pursued in the laboratory and clinic for treatment of various diseases, their application to growing tissues is limited by their fixed shapes. Stretchable multielectrode arrays have been used to map the electrophysiological signal on an actively beating heart without mechanical failure or sensor dislocation[9,10]. Intrinsically stretchable neurological devices have shown improved biocompatibility and seamless interaction with both the peripheral nervous system[11] and the central nervous system[12]. Even though elastic bioelectronics can accommodate repeated strain induced by the dynamics of organ and body movement, challenges remain in adapting to developmental tissue growth without asserting substantial stress during the process. For example, implantable vagus nerve stimulators, which can be highly effective in reducing seizure occurrence in some patients with drug-resistant epilepsy (accounting for 30% of total epilepsy population), is frequently used off-label in young children (<12 years old), with serious issues of tissue restriction and associated side effects[6,13,14].

Here we develop morphing electronics (MorphE), which have growth-adaptive properties and require a fundamentally different design from previous stretchable electronics. First, permanent deformation is induced only by slow tissue growth, not by fast body movement and therefore a strain-rate-dependent mechanical response is needed. Second, the device should adapt and morph while exerting minimal stress on the interfaced tissue during growth. Furthermore, large variation in organ size from person to person demands reconfigurable electronics that can be adjusted to arbitrary shapes during surgery. Based on these requirements, electronics that undergo irreversible deformations, rather than elastic electronics, are desired for reconfigurable implantation procedures and reduction in tissue constraint for growing organs.

In this work, we designed and implanted a MorphE on the sciatic nerve of rapidly growing rats (Fig. 1a,b). The key materials for MorphE include a viscoplastic conductive polymer and an insulating and self-healable viscoplastic polymer (VP). Biocompatible glycerol is used to introduce disorder[15,16] and modulate the mechanical properties, while maintaining high conductivity (Supplementary Fig. 1) of the conductive polymer, poly(3,4-ethylenedioxythiophene) polystyrene sulfonate (PEDOT:PSS). The PEDOT:PSS/glycerol conductor showed only a 3.9-times increase in resistance when stretched to 100% strain (Fig. 1c). In contrast, without adding glycerol, PEDOT:PSS showed a more than 30-times increase in resistance under 8% uniaxial strain. To achieve the desired self-healing and viscoplastic properties (Supplementary Fig. 2), we fine-tuned the ratio between the weak dynamic bonding isophorone bisurea (IU) units and strong hydrogen bonding 4,4′-methylenebis(phenyl urea) (MPU) units in VP by blending poly(dimethylsiloxane) (PDMS)–IU with PDMS–$IU_{0.6}$–$MPU_{0.4}$ (Supplementary Notes).

In contrast to a previous viscoelastic polymer design[17], modulating the ratio of IU and MPU to 7:3 allowed an irreversible plastic deformation of MorphE at 100% uniaxial strain (Fig. 1b and Supplementary Fig. 3). The PEDOT:PSS/glycerol/VP showed typical viscoelastic behavior at strain rates higher than 5% s^{-1} and zero stress at a lower strain rate of 0.05% s^{-1}, suggesting that there is no mechanical constraint applied to the sciatic nerve at a normal growth rate (~2×10^{-5}% s^{-1}; Fig. 1d).

Tensile stress responses at different strain rates revealed the strain-rate-dependent mechanical properties of the viscoplastic device. Specifically, the device behaved like a 'flowable liquid' at a strain rate similar to the tissue growth rate, but behaved like a solid at higher strain rates, which can help to prevent unintended

[1]Department of Bioengineering, Stanford University, Stanford, CA, USA. [2]Department of Chemical Engineering, Stanford University, Stanford, CA, USA. [3]Department of Neurology and Neurological Sciences, Stanford University School of Medicine, Stanford, CA, USA. [4]Department of Chemistry, Stanford University, Stanford, CA, USA. [5]Department of Materials Science and Engineering, Stanford University, Stanford, CA, USA. [6]Stanford Stroke Center and Stanford University School of Medicine, Stanford, CA, USA. [7]Present address: Department of Materials Science and Engineering, Korea Advanced Institute of Science and Technology (KAIST), Daejeon, Republic of Korea. [8]These authors contributed equally: Yuxin Liu, Jinxing Li, Shang Song. [9]These authors jointly directed this work: Paul M. George, Zhenan Bao. ✉e-mail: pgeorge1@stanford.edu; zbao@stanford.edu

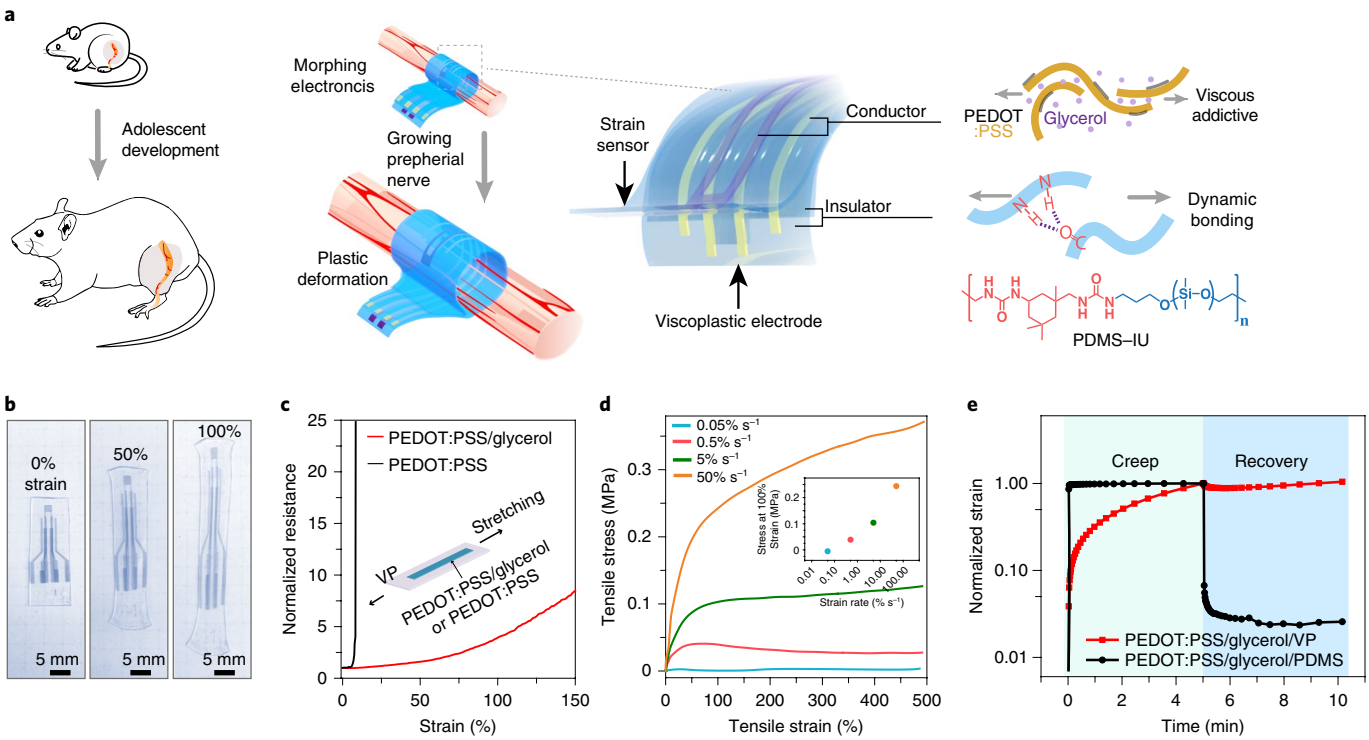

Fig. 1 | MorphE using viscoplastic electronic materials. a, Schematics showing adolescent development of the rat and the MorphE that conformally adapts to sciatic nerve growth. The MorphE is composed of two materials: PEDOT:PSS plasticized by a viscous additive (glycerol) serving as a soft conductor and a polymer blend of PDMS-IU and PDMS-$IU_{0.6}$-$MPU_{0.4}$ as a viscoplastic insulator. MorphE allows plastic deformation with little stress when stretched by a growing nerve. **b**, Image of MorphE after being stretched at 50% and 100% strain. It maintains the shape after force is released. **c**, Normalized resistance for untreated PEDOT:PSS (thickness: 2 μm) and PEDOT:PSS/glycerol (thickness: 2 μm) on VP substrate (length, 8 mm; width, 3 mm; thickness, 120 μm) under 150% strain. **d**, Uniaxial stress–strain curves for PEDOT:PSS/glycerol on VP substrate (length, 9 mm; width, 5 mm; thickness, 200 μm) at various strain rates. Stress at 100% strain for various strain rates, showing strain-rate-dependent viscoplastic behavior (inset). **e**, Creep-recovery tests for PEDOT:PSS/glycerol on VP substrate and PEDOT:PSS/glycerol on PDMS substrate. No recovery after force is released for PEDOT:PSS/glycerol/VP (length, 8 mm; width, 5.5 mm; thickness, 200 μm for both samples).

morphological alterations during the implantation procedure and body movement. Even at high strain rates, MorphE causes lower mechanical disturbance to soft tissue, because Young's modulus of MorphE (0.4 MPa measured at a strain rate of 50% s^{-1}) is much lower than that of other implantable soft bioelectronics, such as PDMS-based neural interfaces (1.5 MPa)[12].

At body temperature (37 °C), the degree of plasticity of the VP substrate (Methods) was 97.2%, which is substantially higher than that of a PDMS substrate (2.4%) (Fig. 1e). In the stress relaxation test, the stress in PEDOT:PSS/glycerol/VP decreased below 1% within 236 s, which further demonstrates the quick stress relaxation and excellent viscoplastic properties of MorphE (Supplementary Fig. 4). Substantially lower mechanical constraint on soft tissue was achieved in PEDOT:PSS/glycerol on the VP substrate compared to that on a PDMS substrate (Supplementary Fig. 5). Overall, such material design enables great biocompatibility, high viscoplasticity and close-to-zero stress when the electronic material is subject to a slow strain rate. When the fast strain rate is asserted, in contrast, the material shows elastic properties and allows intimate contact between the electrode and nerve.

MorphE was made by vertical integration of five functional layers including a top insulation layer VP, PEDOT:PSS/glycerol electrodes and interconnects, an intermediate insulation layer VP, a PEDOT:PSS/glycerol-based strain sensor and a substrate VP layer (Supplementary Fig. 6). The developed fabrication method (with a minimal feature size of 150 μm by laser engraving) enabled the combined function of electrical stimulation and strain sensing for nerve diameter monitoring (Supplementary Fig. 7). The self-healing between functional components, together with physical interpenetration between layers (Supplementary Fig. 8), enables a simple and modular fabrication method for multilayered bioelectronics. The 150-μm feature size of conducting PEDOT:PSS electrodes patterned using the laser engraving process is also promising in localized neurophysiological recording and stimulation[11,12,18].

The self-healing mechanism is especially advantageous for surgical procedures because it allows in situ device reconfiguring and reshaping during implantation and thus enables adequate customized fitting without the need for any previous information about the morphology and size of the nerves. In a conventional implantation procedure, the peripheral nerve was slid into a cuff through the slit (Fig. 2a). The large Young's modulus mismatch and stress at the interface between soft nerve and stiff cuff electrode (made of platinum and elastic silicone rubber) can deteriorate nerve functionality[19,20].

Using the self-healing-enabled assembly, we developed a biomechanically compatible, suture-free, individually reconfigurable implantation scheme to allow for a stable and intimate interface between the tissue-like MorphE and the soft sciatic nerve. First, the thin-film device was gently placed underneath the sciatic nerve (Fig. 2b), wrapped around the nerve with a tweezer and subsequently attached to the other side, forming a soft enclosure. The ability to self-heal in an aqueous environment is attributed to the hydrophobic nature of the PDMS backbone in PDMS–IU, and the increased enthalpy gained by strong hydrogen bonding formation described by the previous report[17]. After assembly of MorphE with the sciatic nerve, we observed that repeated pulling of the MorphE device

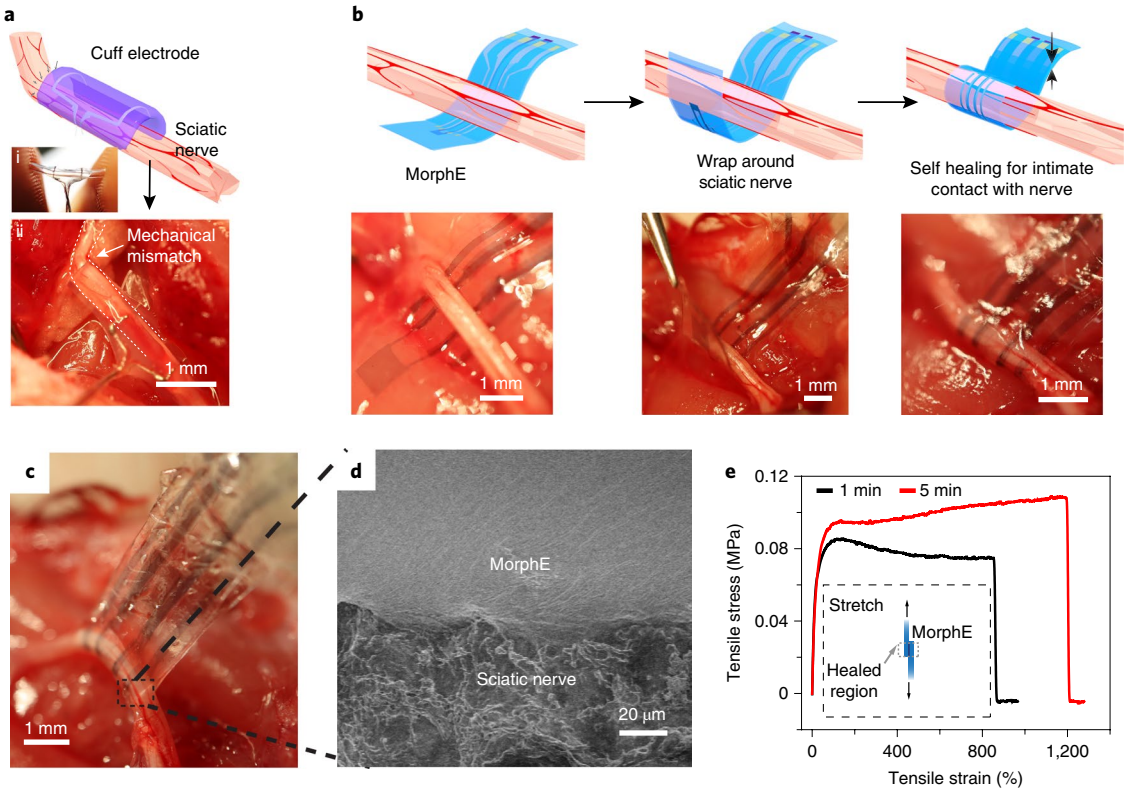

Fig. 2 | Self-bonding MorphE for soft and conformable neural interfaces. a, Schematic showing cuff electrode on sciatic nerve. The photographic images showing rigid cuff held by fingers (i) and nerve deformed by the high-modulus cuff electrodes (ii). Scale bar, 1 mm. **b**, Schematics and images of implantation process for MorphE. Stable enclosure was achieved by wrapping MorphE around the sciatic nerve. Scale bar, 1 mm. **c**, Image of MorphE being pulled by tweezer after 5 min of self-healing, showing a robust neural interface. Scale bar, 1 mm. **d**, SEM image (top) showing an intimate device–nerve interface. Scale bar, 20 μm. **e**, Uniaxial tensile stress–strain curves of two self-healed MorphE at 37 °C in PBS at 5% s^{-1} strain rate. Before the stress–strain test, a 5 × 5 mm^2 overlapped region was attached for 1 and 5 min, respectively to allow self-healing.

caused no visible delamination or dislocation, suggesting a durable nerve interface capable of withstanding physiological movements (Fig. 2c). Scanning electron microscopy (SEM) further confirmed the seamless nerve–device interface after 4 weeks of strain cycles in vivo (Fig. 2d). With only 1 min of self-healing at 37 °C in phosphate-buffered saline (PBS), the bonded sample sustained 858% strain at a strain rate of 5% s^{-1} (Fig. 2e).

To ascertain the chronic stability of implanted MorphE, its electrochemical impedance and cathode charge storage capacity (CSCc) were measured over 8 weeks of soaking in PBS. We observed that the impedance of MorphE was substantially lower than that of a standard cuff electrode (Supplementary Fig. 9) and remained relatively stable over the entire soaking period (Fig. 3a and Supplementary Fig. 10), though the biocompatible glycerol partially diffused out (weight percentage of glycerol decreased by 11%; Supplementary Fig. 11). The high CSCc of the MorphE is derived from: (1) the dual conductive nature (both electronically and ionically conductive) of PEDOT:PSS; (2) nanoporous structure of PEDOT:PSS enables high volumetric capacitance; and (3) the interconnect volume further reduces the interfacial impedance without changing the electrode surface area as the electrolyte diffuses into the polymeric interconnect[11,21]. In addition, MorphE showed strain-insensitive impedance and maintained a relatively stable resistance in a repeated stretch-and-release cycling test (Supplementary Figs. 11–13).

A higher CSCc is desirable for larger charge injection at a given stimulation voltage. The CSCc showed a slight increase until week 2 due to decreased impedance and then stabilized at 137.0 ± 7.7 mC cm^{-2}, which is much higher than that of cracked Au (46.9 ± 3.3 mC cm^{-2})[12] and electrochemically deposited PEDOT (75.6 mC cm^{-2})[22]. Next, the impedance through the VP insulation layer was measured at ~26 MOhm (at 1 kHz), which is substantially higher than the electrode impedance of 6.3 kOhm (at 1 kHz) (Supplementary Fig. 14), indicating a low leakage current from the insulated area and high insulation capacity.

To examine device performance during tissue development, we performed animal studies selecting the fastest growing period in rats. From week 0 to week 4 postimplantation, the measured average sciatic nerve diameter increased 140% from approximately 0.5 ± 0.03 mm to 1.2 ± 0.1 mm and the rat average weight increased by 107% from 144 ± 9 g to 299 ± 4 g. Thereafter, the growth of the nerve diameter plateaued from week 4 to week 8 (Supplementary Fig. 15). A resistive strain sensor was used to monitor expansion of nerve diameter. We observed the expected steady increase in resistance as the nerves grew. The diameter changes, calculated based on measurements from the strain sensor, showed a close match with actual nerve diameter changes (Fig. 3b). Both the implanted MorphE and the commercial cuff electrode successfully evoked compound action potential (CAP) immediately after implantation. However, the MorphE showed a substantially higher peak-to-peak CAP amplitude than that of the cuff electrodes (Supplementary Fig. 16). Due to dual conduction of electrons and ions in PEDOT:PSS/glycerol and the porous interconnect fabricated through the use of a conductive polymer[11], a low threshold voltage of 100 mV is sufficient to evoke a CAP with MorphE (Fig. 3c). In contrast, 300 mV was required for the cuff electrode to evoke detectable responses.

Next, we carried out electrophysiological measurements throughout the adolescent developmental process of rats. The CAP was observed to be evoked after implantation from week 0 to week 8 for

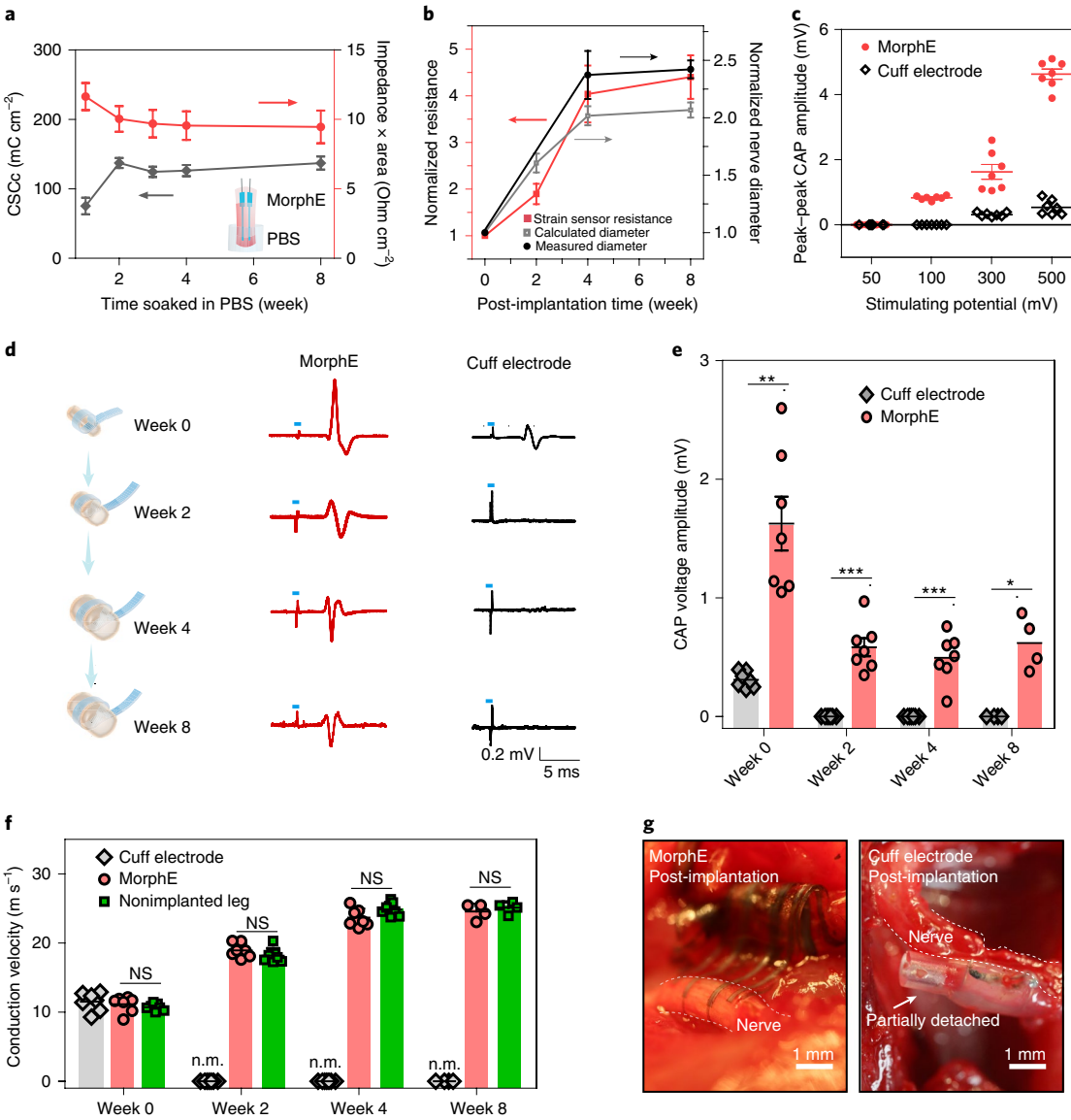

Fig. 3 | MorphE accommodates developmental growth for chronically stable neuromodulation, nerve growth monitoring and conduction velocity testing. a, CSCc and impedance × area (at 1 kHz) for MorphE ($n=3$) soaked in PBS at 37 °C for 8 weeks. The electrode size is 0.04 cm^2. Inset: schematics showing the MorphE immersed in PBS. **b**, Normalized resistance changes over 8-week implantation. The normalized nerve diameter was calculated based on the strain–resistance curve and compared to measured nerve diameter ($n=3$ for week 0 to 4 and $n=4$ for week 8). **c**, Amplitude of evoked CAP on a sciatic nerve with electrical stimulation (voltage amplitude varying from 50 to 500 mV for both cuff electrodes and MorphE). Monophasic pulse (200 μs) at 1 Hz was used. **d**, Representative trace of elicited CAP stimulated by MorphE and cuff electrode for 8 weeks. Blue dash denotes the 200 μs electrical stimulation pulse with amplitude of 300 mV. **e**, Amplitude of CAP change over time for both cuff electrodes and MorphE (week 0, $P=0.0011$; week 2, $P=0.0002$; week 4, $P=0.0006$; week 8, $P=0.012$). **f**, Conduction velocity measured by MorphE, cuff electrodes, compared to that of nonimplanted nerve in growing rats. n.m., not measurable due to device failure. MorphE versus nonimplanted leg (week 0, $P=0.42$; week 2, $P=0.19$; week 4, $P=0.08$; week 8, $P=0.46$). **g**, Image of cuff electrode and MorphE after 4-week implantation. The cuff electrode was outgrown and partially detached from the sciatic nerve. Scale bar, 1 mm. All error bars denote s.d. $^*P<0.05$; $^{**}P<0.01$; $^{***}P<0.001$; NS, not significant; unpaired, two-tailed Student's *t*-test was used for **e** and **f**, $n=7$ (MorphE or cuff electrode) or $n=8$ (sham control) for week 0 to week 4; $n=4$ for week 8.

MorphE with stable neuromodulation performances (Fig. 3d). In contrast, the cuff electrodes could not evoke a detectable CAP after week 2, although electrical stimulation artifacts were recorded (Fig. 3e). We then calculated the conduction velocity, a key indicator for the condition of the peripheral nerve and a biomarker for diseases like carpal tunnel syndrome. We observed a gradual increase in conduction velocity for MorphE-implanted rats (Fig. 3f and Supplementary Fig. 17), which was expected as the nerves grew bigger[23]. In addition, rats implanted with MorphE had similar conduction velocities to nonimplanted nerve from week 0 to week 8 postimplantation.

To investigate why the cuff electrodes failed to evoke CAP, we evaluated the implantation site of the sciatic nerve at week 4. Although suture (and even biocompatible glue) were applied to stabilize the cuff electrode, all the implanted cuff electrodes were observed to have partially detached from the nerve and were unable to suitably accommodate the growth of the peripheral nerve, hence failing their function as chronic monitoring devices. The MorphE ($N=7$) maintained a stable interface for long-term neuromodulation and monitoring (Fig. 3g and Supplementary Video 1). With these results, we demonstrated that MorphE can not only adapt

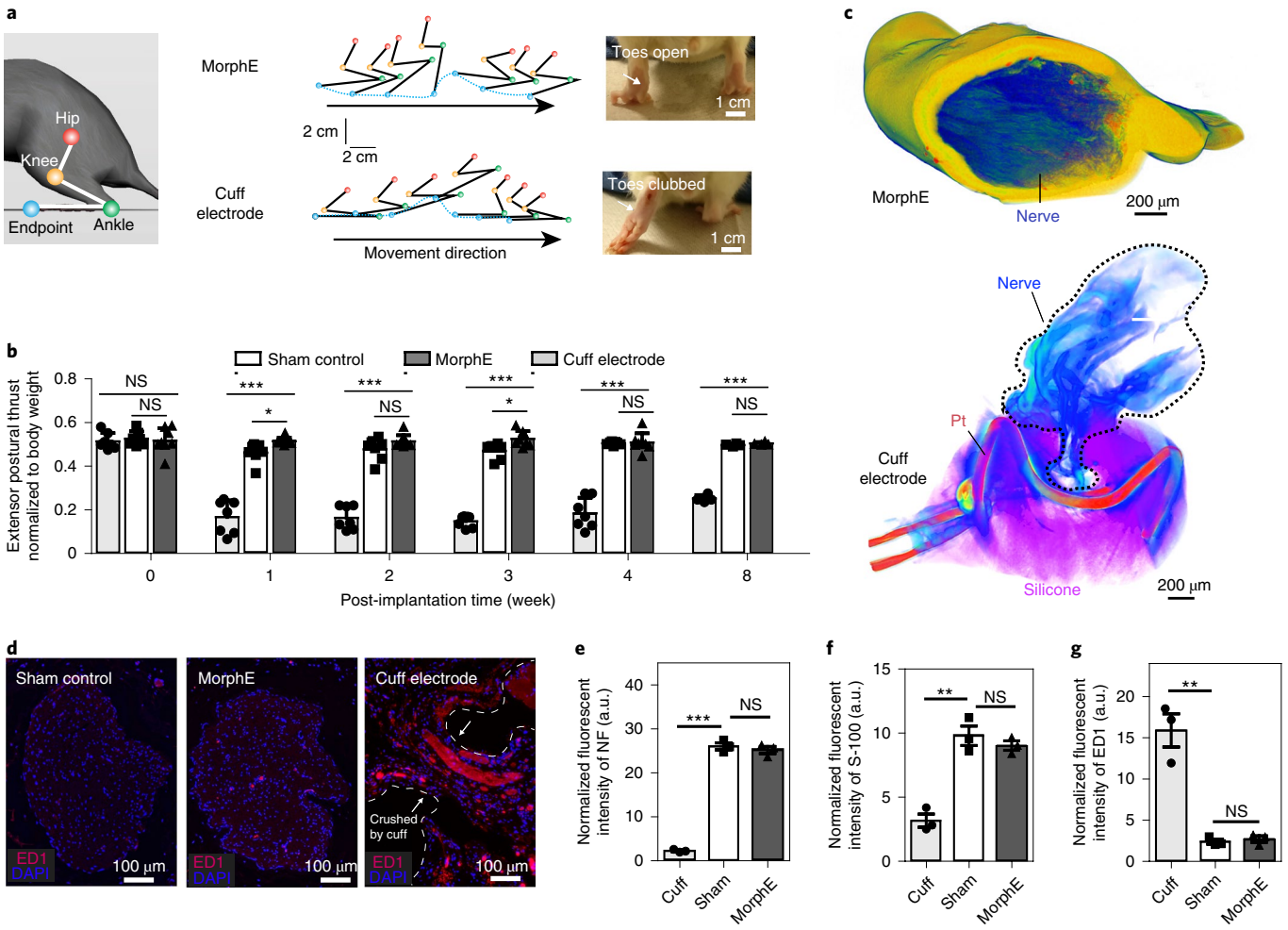

Fig. 4 | Behavior study and biocompatibility of MorphE on growing nerves. a, Hindlimb kinematics during walking (left). Stick diagram decompositions of hindlimb movements (middle). Scale bar, 2 cm. Images of toes for rat implanted with MorphE and cuff electrode (right). Scale bar, 1 cm. **b**, Extensor postural thrust normalized to body weight for rats implanted with MorphE and cuff electrode and sham control from week 0 (before implantation) to week 8; MorphE ($n=7$) and cuff electrodes ($n=7$) were compared to sham control ($n=8$) to calculate P value for week 0 to week 4, $n=4$ for week 8; for MorphE versus sham control: week 0, $P=0.71$; week 1, $P=0.02$; week 2, $P=0.13$; week 3, $P=0.01$; week 4, $P=0.76$; week 8, $P=0.11$; for cuff electrode versus sham control: week 0, $P=0.90$; week 1, $P=1.25\times10^{-5}$; week 2, $P=9.93\times10^{-8}$; week 3, $P=6.46\times10^{-12}$; week 4, $P=1.85\times10^{-6}$; week 8, $P=1.16\times10^{-5}$. Two-tailed Student's t-test was used for data analysis, $^{*}P<0.05$, $^{**}P<0.01$, $^{***}P<0.001$. **c**, Reconstructed three-dimensional μCT scans of the sciatic nerve after chronic implantation of MorphE and cuff electrode. Scale bar, 200 μm. **d**, Cross-sectional slice of sciatic nerve labeled by the inflammatory biomarker ED1 for MorphE, cuff electrodes and sham control. DAPI, 4′,6-diamidino-2-phenylindole. Three experiments were repeated independently with similar results. Scale bar, 100 μm. **e**–**g**, Histogram showing normalized fluorescence intensity of neurofilaments (**e**), S-100 (**f**) and ED1 (**g**) for MorphE, cuff electrodes and sham control. For neurofilament: MorphE, $P=0.49$;cuff electrode, $P=8.8\times10^{-6}$; for S-100: MorphE, $P=0.42$; cuff electrode, $P=0.0019$; for ED1: MorphE, $P=0.58$; cuff electrode, $P=0.0027$; $^{**}P<0.01$, $^{***}P<0.001$ ($n=3$, unpaired, two-tailed Student's t-test). All error bars denote s.d. a.u., arbitrary units.

to tissue growth but can also maintain stable strain-sensing and neuromodulation in growing rats. The stable and conformable interface between MorphE and the nerve after chronic implantation also indicates that the daily motion of the animal, usually at a very high strain rate, would not cause undesired deformation of the device.

To determine whether and how MorphE impacts the growing rat, we next investigated gait, behavior changes, structural damages and immune response during adolescent rat growth. Rats implanted with MorphE showed normal gait[24], with their walking observed with normal paw placement and toes spread (Fig. 4a and Supplementary Fig. 18). However, rats with implanted cuff electrodes experienced abnormal paw function with whole-foot placement on the ground and dragging of their toes (Supplementary Video 2), a typical symptom of serious sciatic nerve dysfunction[24].

With regard to objective measures of sciatic nerve injury, a battery of sensory and motor tests was performed[25]. MorphE-implanted rats exhibited normal nociception to hot temperatures compared to the severe sensing dysfunction displayed in rats implanted with cuff electrodes. (Supplementary Fig. 19 and Supplementary Notes). A series of motor tests further demonstrated that MorphE-implanted rats retained natural motor function, whereas cuff-electrode-implanted rats suffer from permanently reduced motor responses (Fig. 4b and Supplementary Fig. 19) After 8 weeks of implantation, the normalized extensor postural thrust showed a 51.5% force reduction for the cuff electrode, whereas there was only a 5.5% change for MorphE.

Next, reconstructed three-dimensional microcomputed tomography (μCT) revealed that MorphE seamlessly and conformably interfaced with the sciatic nerve (Fig. 4c). In contrast, the inner

diameter of the cuff electrode was observed to have been outgrown by the sciatic nerve, leading to structural deformation of the peripheral nerve. It is worth noting that mechanical constraint did not only occur at the interface between nerve tissue and platinum electrode. The μCT revealed that the silicon-based elastic substrate also severely constrained and damaged the nerve tissue (Supplementary Fig. 20). There was no statistically significant difference ($P=0.49$, $P=0.42$ and $P=0.58$, respectively) in expression levels of the neurofilaments, S-100 (a marker for Schwann cells; Supplementary Figs. 21 and 22) and ED1 (a marker for inflammatory response) biomarkers between MorphE-implanted nerves and sham controls. In contrast, S-100 and neurofilament for cuff-implanted nerves had significantly ($P=0.0019$ and $P=8.8\times10^{-6}$, respectively) lower expression level compared to sham controls, whereas ED1 had significantly ($P=0.0027$) higher expression in cuff-implanted nerves (Fig. 4d–g and Supplementary Fig. 23). Masson's trichrome staining tests further showed that implanted cuff electrodes severely crushed the rat's nerves, leading to disintegration of epineurium, increased number of blood vessels and reduced size of fascicles (Supplementary Fig. 24). These results suggest that mechanical stress due to implant detachment and 'chronic compression' as opposed to an initial crush injury are likely to be the underlying mechanisms[26–30]. Together, gait, behavior, structural and histology results all supported that MorphE is able to suitably accommodate nerve growth with minimal negative influence on growing rats.

In conclusion, through the development of viscoplastic and self-healable electronic material, we fabricated a chronic and neurologically implantable morphing electronic device (MorphE) capable of actively adapting to in vivo tissue growth. The self-healing properties of the materials were used for assembly of multilayered polymeric electronics and for reshaping the MorphE device structure to fit anatomic morphology, creating a robust device–tissue interface. MorphE device demonstrated the feasibility of neuromodulation and strain sensing with minimal tissue constraint in developing rats.

We envision that integrating MorphE with wireless electronics could enable therapeutic modulation in treating chronic neurological disorders. High-resolution fabrication of electrodes will allow selective neurostimulation and enable integration of recording and stimulation that is critical for closed-loop neuromodulation. A new viscoplastic material system for human use will require stable operation in body tissue for years. To achieve this, we need further in vivo investigation beyond 2 months and strategies to prevent diffusion of the plasticizer from the viscoplastic conductor.

Translation of the growth-adapting concept in designing future pediatric implantable electronics would confer impactful benefits to young patients with improved efficacy and reduced complication rates. The viscoplastic design with minimal disturbance of developing tissues will also enable development of new functional tools to interrogate physiological processes that originate, shape and re-shape, the nervous system from embryonic development to adulthood.

Online content

Any methods, additional references, Nature Research reporting summaries, source data, extended data, supplementary information, acknowledgements, peer review information; details of author contributions and competing interests; and statements of data and code availability are available at https://doi.org/10.1038/s41587-020-0495-2.

Received: 13 September 2019; Accepted: 16 March 2020;
Published online: 20 April 2020

References

1. Jonsson, A. et al. Therapy using implanted organic bioelectronics. *Sci. Adv.* **1**, e1500039 (2015).
2. Borovikova, L. V. et al. Vagus nerve stimulation attenuates the systemic inflammatory response to endotoxin. *Nature* **405**, 458–462 (2000).
3. Johnson, R. L. & Wilson, C. G. A review of vagus nerve stimulation as a therapeutic intervention. *J. Inflamm. Res.* **11**, 203–213 (2018).
4. Borzage, M., Blüml, S. & Seri, I. Equations to describe brain size across the continuum of human lifespan. *Brain Struct. Funct.* **219**, 141–150 (2014).
5. Meier, J. M. et al. Assessment of age-related changes in abdominal organ structure and function with computed tomography and positron emission tomography. *Semin. Nucl. Med.* **37**, 154–172 (2007).
6. Samuels-Reid, J. H. & Cope, J. U. Medical devices and adolescents: points to consider. *JAMA Pediatr.* **170**, 1035–1036 (2016).
7. Samdani, A. F. et al. Anterior vertebral body tethering for immature adolescent idiopathic scoliosis: one-year results on the first 32 patients. *Eur. Spine J.* **24**, 1533–1539 (2015).
8. Aalbers, M. W., Rijkers, K., Klinkenberg, S., Majoie, M. & Cornips, E. M. J. Vagus nerve stimulation lead removal or replacement: surgical technique, institutional experience, and literature overview. *Acta Neurochir.* **157**, 1917–1924 (2015).
9. Lee, W. et al. Nonthrombogenic, stretchable, active multielectrode array for electroanatomical mapping. *Sci. Adv.* **4**, eaau2426 (2018).
10. Xu, L. et al. 3D multifunctional integumentary membranes for spatiotemporal cardiac measurements and stimulation across the entire epicardium. *Nat. Commun.* **5**, 3329 (2014).
11. Liu, Y. et al. Soft and elastic hydrogel-based microelectronics for localized low-voltage neuromodulation. *Nat. Biomed. Eng.* **3**, 58–68 (2019).
12. Minev, I. R. et al. Electronic dura mater for long-term multimodal neural interfaces. *Science* **347**, 159–163 (2015).
13. Aaberg, K. M. et al. Short-term seizure outcomes in childhood epilepsy. *Pediatrics* **141**, e20174016 (2018).
14. Peña, C., Bowsher, K. & Samuels-Reid, J. FDA-approved neurologic devices intended for use in infants, children, and adolescents. *Neurology* **63**, 1163–1167 (2004).
15. Wang, Y. et al. A highly stretchable, transparent, and conductive polymer. *Sci. Adv.* **3**, e1602076 (2017).
16. Savagatrup, S., Printz, A. D., O'Connor, T. F., Zaretski, A. V. & Lipomi, D. J. Molecularly stretchable electronics. *Chem. Mater.* **26**, 3028–3041 (2014).
17. Kang, J. et al. Tough and water-insensitive self-healing elastomer for robust electronic skin. *Adv. Mater.* **30**, e1706846 (2018).
18. Khalifa, A. et al. The microbead: a 0.009 mm^3 implantable wireless neural stimulator. *IEEE Trans. Biomed. Circuits Syst.* **13**, 971–985 (2019).
19. O'Brien, J. P. et al. A model of chronic nerve compression in the rat. *Ann. Plast. Surg.* **19**, 430–435 (1987).
20. Restaino, S. M., Abliz, E., Wachrathit, K., Krauthamer, V. & Shah, S. B. Biomechanical and functional variation in rat sciatic nerve following cuff electrode implantation. *J. Neuroeng. Rehabil.* **11**, 73 (2014).
21. Rivnay, J., Wang, H., Fenno, L., Deisseroth, K. & Malliaras, G. G. Next-generation probes, particles, and proteins for neural interfacing. *Sci. Adv.* **3**, e1601649 (2017).
22. Wilks, S. Poly(3,4-ethylene dioxythiophene) (PEDOT) as a micro-neural interface material for electrostimulation. *Front. Neuroen.* **2**, 7 (2009).
23. Cragg, B. G. & Thomas, P. K. The relationships between conduction velocity and the diameter and internodal length of peripheral nerve fibres. *J. Physiol.* **136**, 606–614 (1957).
24. de Medinaceli, L., Freed, W. J. & Wyatt, R. J. An index of the functional condition of rat sciatic nerve based on measurements made from walking tracks. *Exp. Neurol.* **77**, 634–643 (1982).
25. Kohane, D. S. et al. A re-examination of tetrodotoxin for prolonged duration local anesthesia. *Anesthesiology* **89**, 119–131 (1998).
26. Nitz, A. J., Dobner, J. J. & Matulionis, D. H. Structural assessment of rat sciatic nerve following tourniquet compression and vascular manipulation. *Anat. Rec.* **225**, 67–76 (1989).
27. Dyck, P. J., Lais, A. C., Giannini, C. & Engelstad, J. K. Structural alterations of nerve during cuff compression. *Proc. Natl Acad. Sci. USA* **87**, 9828–9832 (1990).
28. Beel, J. A., Groswald, D. E. & Luttges, M. W. Alterations in the mechanical properties of peripheral nerve following crush injury. *J. Biomech.* **17**, 185–193 (1984).
29. Rydevik, B., McLean, W. G., Sjöstrand, J. & Lundborg, G. Blockage of axonal transport induced by acute, graded compression of the rabbit vagus nerve. *J. Neurol. Neurosurg. Psychiatry* **43**, 690–698 (1980).
30. Bora, F. W., Richardson, S. & Black, J. The biomechanical responses to tension in a peripheral nerve. *J. Hand Surg. Am.* **5**, 21–25 (1980).

Methods

Preparation of PEDOT:PSS/glycerol. PEDOT:PSS Orgacon ICP 1050 was provided by Agfa as a surfactant-free aqueous dispersion with 1.1 wt% solid content. The PEDOT:PSS dispersion was filtered through a 1.0-μm filter to remove any potential large agglomerates before use. Glycerol (G9012-100ML) was purchased from Sigma-Aldrich. Different ratios of the dry weight of PEDOT:PSS and glycerol were used from 1:1 to 1:32. Glycerol was added to the filtered PEDOT:PSS aqueous solution and stirred vigorously at room temperature for 20 min. The PEDOT:PSS/glycerol aqueous mixture was then filtered through a 0.45-μm syringe filter. For thin film preparation, the filtered PEDOT:PSS/glycerol solution was spin coated on a glass substrate at a speed of 400 r.p.m. for 1 min, followed by drying for 4 h at room temperature. The glass substrates were oxygen plasma (Technics Micro-RIE Series 800) treated at 150 W for 45 s before spin coating. Alternatively, the film could be obtained by drop-casting the PEDOT:PSS/glycerol aqueous mixture and drying at room temperature overnight.

Synthesis of PDMS–IU and PDMS–$IU_{0.6}$–$MPU_{0.4}$. The synthetic procedures of PDMS–MPU_x–IU_{1-x} ($x = 0$ and 0.4) were reported previously[17]. The polymers were synthesized through a one-pot polycondensation reaction between bis(3-aminopropyl)-terminated poly(dimethylsiloxane) (H_2N–PDMS–NH_2, number-averaged molecular weight $M_n = 5{,}000$, from Gelest) and a mixture of 4,4′-methylenebis(phenyl isocyanate) and isophorone diisocyanate. As a result, the PDMS oligomers (PDMS–MPU_x–IU_{1-x}) were linked by an MPU unit and IU unit with different ratios of MPU and IU units. Four grams of the synthesized PDMS–$MPU_{0.4}$–$IU_{0.6}$ (weight-averaged molecular weight $M_w = 116{,}000$; $M_n = 73{,}000$, dispersity $Đ = 1.6$) and PDMS–IU ($M_w = 123{,}000$; $M_n = 68{,}000$, $Đ = 1.8$) were dissolved in 20 ml of toluene in two separate vials and stirred at 50 °C. The resultant viscous solution was stirred for more than 3 h and was subsequently gradually cooled to room temperature. Then, PDMS–$MPU_{0.4}$–$IU_{0.6}$ (in toluene) was blended with PDMS–IU (in toluene) with a volume ratio of 0:1, 1.5:1 and 3:1.

Device fabrication. The PEDOT:PSS/glycerol film (weight ratio of 1:32) on glass substrate was laser-engraved by Epilog Fusion M2 laser. The electronic design was created with CorelDraw software. A CO_2 laser with 30% power and 20% speed was used. VP polymers (20 wt% in toluene) were then drop casted on the PEDOT:PSS/glycerol pattern and dried in ambient conditions overnight and heated in an oven at 70 C° for 2 h to facilitate the physical interpretation between VP and PEDOT:PSS/glycerol. The PEDOT:PSS/glycerol patterns, including electrodes and strain sensor, were transferred onto VP. The silicone rubber-insulated thin wire cut from the cuff electrode (World Precision Instruments) were connected to the electrodes and strain sensor using conductive epoxy (CW2500, Chemtronics). Finally, the electrode layer, strain sensor layer and top insulating VP layer were aligned under a stereomicroscope. All the layers self-healed into multilayered MorphE through hydrogen bonding between VP materials.

Conductivity characterization. Freestanding PEDOT:PSS/glycerol film was measured using the direct current four-point probe method with a Keithley 2400 Source meter at room temperature. The width and length of the film were measured by a caliper. The thickness was measured with a micrometer or an optical microscope.

Morphological and compositional characterization. SEM imaging was carried out on an FEI Magellan 400L XHR SEM. Elemental composition mapping was performed using an energy dispersive X-ray detector coupled to the SEM. To obtain the molecular weight of PDMS–IU (VP1) and PDMS–$IU_{0.6}$–$MPU_{0.4}$ (VP2), analytical gel permeation chromatography experiments were performed on a Malvern VE2001 gel permeation chromatography solvent/sample module with three ViscoGELTM I-MBHMW-3078 columns. A three-dimensional laser scanning microscope (Keyence, VK) was used to characterize the thickness change before and after 2 months of soaking.

Mechanical characterization. PEDOT:PSS/glycerol aqueous solutions were directly spin coated onto a plasma-treated PDMS substrate at 400 r.p.m. for 1 min. PEDOT:PSS/glycerol was spin coated onto glass at 400 r.p.m. for 1 min and subsequently transferred to VP. A rheometer (TA Instruments, ARES-G2) was used to characterize the mechanical properties for both PEDOT:PSS/glycerol/VP and PEDOT:PSS/glycerol/PDMS. Samples were cut into 8-mm diameter disks to match the plate diameter. The rheological measurement was performed with a frequency sweep measurement from 10 Hz to 0.001 Hz. Creep-recovery tests were also performed to assess the degree of plasticity for PEDOT:PSS/glycerol on the VP substrate compared to PEDOT:PSS/glycerol on a PDMS substrate by the following equation: the degree of plasticity $= \frac{\varepsilon_i}{\varepsilon_{max}}$, where ε_i is the irreversible strain after recovery and ε_{max} is the maximum strain at the end of the creep test[31]. Dynamic mechanical analysis (TA Instruments, Q800) was used to characterize PEDOT:PSS/glycerol/VP and PEDOT:PSS/glycerol/PDMS at 37 C°. Constant stress was applied for 300 s while the strain was measured over time. Stress was continuously monitored for 300 s after removing the stress. Stress relaxation and stress–strain curves were obtained by using an Instron tensile testing system (Instron, 5565). To investigate the strain-rate mechanical dependency, strain rates of 0.05% s^{-1}, 0.5% s^{-1}, 5% s^{-1} and 50% s^{-1} were applied with Instron. Freshly collected rat muscle was cut into thin slices of 4.6 mm width × 6.8 mm length × 1.1 mm thickness. PEDOT:PSS/glycerol/PDMS and PEDOT:PSS/glycerol/VP with the same width and length (thickness of 120 μm, in which PEDOT:PSS/glycerol thickness was 2 μm) were interfaced with muscle slices, respectively. The Instron was used to characterize the stress–strain response for muscle, muscle/PEDOT:PSS/glycerol/PDMS and muscle/PEDOT:PSS/glycerol/VP.

Electrical and electrochemical characterization. To measure the resistance during stretching, samples were attached to a homemade stretching station attached to an LCR meter (Keysight Technologies, E4980). Liquid metal EGaIn was used to make contact. Electrochemical impedance and cyclic voltammetry (CV) were measured with a potentiostat (Biologic VSP-300 workstation and Palm Sens 3) while the sample was immersed in the PBS buffer solution. CV was used to calculate the CSCc. The potentiostatic electrochemical impedance spectroscopy was measured with a sine wave (frequency from 1 Hz to 1 MHz) and a signal amplitude of 10 mV. The CV was performed at a scan rate of 20 mV s^{-1} versus Ag/AgCl (3 M KCl) reference electrode from −0.6 to 0.8 V. Insulation capacity was performed by measuring the electrochemical impedance through an electrode that was fully insulated by VP.

Implantation of MorphE on rat sciatic nerves. The soft peripheral nervous system is a desirable organ system for soft and conductive polymer-based electronic devices[32,33]. All procedures involving implantation and collecting of electrodes on rat sciatic nerves were performed in accordance with protocols approved by the Institutional Animal Care and Use Committee at Stanford University. Surgical procedures were described by a previously published protocol[34] with some modifications. Male Sprague Dawley rats (50–150 g, Charles River) were given buprenorphine 0.1 mg per kg body weight intramuscularly before anesthesia and then anesthetized with 2% isoflurane in balanced oxygen. Under sterile conditions with external body warming, a 3-cm incision was made on the left thigh. About 1 cm of the sciatic nerve proximal to the tibial and peroneal bifurcation was either (1) inserted into the nerve cuff electrode (NS-NC-0.5-2-100PT-3-3-00-300-00, World Precision Instruments) or (2) wrapped with the MorphE. Muscle layers were closed with 4-0 silk sutures (Ethicon) and the skin was secured with Michel clips. At the end of week 4 or week 8 after surgery, rats were killed with carbon dioxide gas followed by decapitation for proper disposal. Sciatic nerves were collected for analysis.

Animal behavior analysis. Animals were divided into matched groups and behavioral testing was performed by double-blinded individuals. Animals were trained on 3 separate days before recording baseline behavior. After implantation, weekly behavior testing such as thermal nociception, extensor postural thrust and positional placing was assessed based on previously published protocols[25,35,36]. Thermal nociception was assessed using a hot plate, where hind paws were exposed to a temperature of 56 °C and the time (thermal latency) that the animal left its paw was measured with a stopwatch. The paw was removed by the experimenter after 12 s to prevent injury to the animal or the development of hyperalgesia. Although the sensation of the lateral foot is mediated by the sciatic nerve, the hip and knee flexion necessary to remove the foot from the hot plate is mediated by the femoral nerve. Therefore, this test was specific for the nociceptive block. Extensor postural thrust measures the maximum weight that the rat could bear without its ankle touching the balance. The rat was held with its posterior placed above a digital balance on which it could bear weight with one hind paw at a time. Positional placing response was used to measure proprioception. A prone rat will respond to having its hind paw pulled back (with the dorsum in contact with the table surface by returning it to a position alongside its flank, with the claws splayed (score of 1) and severe defects resulting in the limb trailing behind the rat with the claws clubbed (score of 4)). If the foot is returned fully to the flank but the digits are clubbed, the score is 2. Any other outcome (for example, the foot is left out at an angle) yielded a score of 3. Hopping was an integrative test of sensory, proprioceptive and motor function. Rats were held above a horizontal surface in the hands of an experimenter so that only one foot could touch the surface. Under this circumstance, a rat will hop when its body is slowly moved laterally. It will not do so if there is a sensory or motor block. The animal was scored between 0 and 1 according to whether the animal could hop. Stick diagram decomposition of hindlimb movements was plotted based on the video, in which the rats are walking on a flat surface.

Electrical stimulation and strain sensing in vivo. Electrophysiology was conducted at weeks 0, 2, 4 and 8 posttransplantation to collect electrical signals from sciatic nerves with implanted devices based on previously published protocols with modifications[37–40]. Rats were anesthetized with 2% isoflurane in balanced oxygen under sterile and body-temperature warming conditions. Wires from implanted devices were retrieved under the skin and connected to the external stimulator (33210A, Keysight). The needle recording electrodes (stainless steel, length of 12.7 mm and diameter of 0.3 mm, BD Precision) were inserted into the ventral side of the rat hind paw of the stimulated leg. Amplifier gain was set at 1,000 with the output of the amplifiers bandpass filtered at 300 Hz to 10 kHz.

Electrophysiological recording was conducted with the leg in a natural relaxed position to prevent any restriction of movement. Amplified potentials were recorded using Labchart (Powerlab, AD Instrument). Stimuli were delivered in the form of constant voltage pulses with intensity from 0 to 1 V and every 1 s to gradually elicit nerve responses. CAPs were continuously recorded before and after stimulation and responses were saved to data files. The distance between stimulating and recording electrodes was measured. The conduction velocity and voltage amplitude were calculated based on a previously published method[40]. We calculated the conduction velocity, a key indicator for the condition of the peripheral nerve and a biomarker for diseases such as carpal tunnel syndrome, by using stimulation-recording distance divided by artifact-to-CAP latency. The resistance of the strain sensor was measured by digital multimeter (dm6450, Sperry Instruments). By fitting the resistance change to the resistance–strain calibration curve, the increase in diameter of the sciatic nerve was calculated. The resistance and diameter of the nerve were normalized to the initial value at week 0. For animal behavior analysis, electrical stimulation and strain-sensing experiments, two batches of rats were used. Rats from the first batch ($n=3$ for MorphE, $n=3$ for cuff electrode, $n=4$ for sham control) were killed at week 4. Rats from the second batch ($n=4$ for MorphE, $n=4$ for cuff electrode, $n=4$ for sham control) were killed at week 8.

Immunohistology and immunostaining. Biocompatibility studies were performed to compare nerve damage and immune responses at the implantation site for MorphE, cuff electrode and sham control. Three rats were used per study group. The rats were killed 4 weeks after implantation. The implanted nerve and sham-operated nerve were fixed in a PBS solution with 4 wt% formaldehyde for 24 h, followed by 70% ethanol for 24 h. Nerves along with implants were collected based on the previous protocol[34,41]. Briefly, samples were embedded in paraffin and sectioned into 4-μm thick slices. After deparaffinization, endogenous peroxidase was blocked with 3% hydrogen peroxide. Antigen retrieval was performed in a microwave using Antigen Target Retrieval Solution (pH 6) (Agilent Technologies) heated to 100 °C for 10 min. H&E and Masson's trichrome staining was conducted following a standard protocol[42]. Briefly, for H&E staining, samples were hydrated and stained with H&E followed by extensive water washes. Similarly, samples were hydrated and treated with Bouin's solution, Weigert's working hematoxylin, Biebrich scarlet acid fuchsin, phosphotungstic/phosphomolybdic acid and aniline blue for Masson's trichrome staining. All steps were followed by dehydration in graded ethanol to xylene. Glass coverslips were applied using a resinous mounting medium (Thermo Fisher Scientific). Neurofilament and S-100 protein in the tissue slices were stained for imaging. The slices were washed with PBS three times and then permeabilized by 0.1% Triton-X 100 in PBS for 15 min. After washing with PBS solution, the samples were incubated in blocking solution (3% bovine serum albumin, 0.1% Triton-X 100 in PBS) for 45 min. The samples were then co-stained with 1:100 dilution anti-S-100 (ab52642, Abcam) and 1:1,000 dilution anti-neurofilament (ab8135, Abcam) in blocking solution overnight at 4 °C. The samples were washed with PBS and stained with secondary antibody anti-rabbit IgG H&L (Alexa Fluor 488, ab150077) and anti-mouse IgG H&L (Alexa Fluor 647, ab150115). Anti-ED1 (MAB1435, Millipore Sigma, 1:200 dilution) were used to characterize inflammatory responses. Epifluorescence and confocal images of samples were taken using a Keyence BZ-X710 microscope equipped with full BZ acquisition and analysis software. Fluorescence intensity was normalized to the mean value of sham control. Unpaired, two-tailed Student's *t*-tests were performed using Prism.

Microcomputed tomography. Sciatic nerves with implants were collected from rats 4 weeks after implantation. To increase contrast, phosphotungstic acid (Sigma-Aldrich 79690–25 G) was used to stain the nerve, followed by freeze drying. Nondestructive computed tomography reconstructions of the implanted sciatic nerve were performed with a Zeiss Xradia 520 Versa X-ray microscope (Carl Zeiss AG). The exposure time of 10 s was used with an acceleration voltage of 40 kV. Projection images were reconstructed into three-dimensional images and processed using Dragonfly software (Object Research Systems).

Statistical analysis. R, Origin, Prism and Excel were used for all statistical analyses. All replicate numbers, error bars, *P* values and statistical tests are indicated in figure legends.

Reporting Summary. Further information on research design is available in the Nature Research Reporting Summary linked to this article.

Data availability

All data are available in the article or Supplementary Information.

References

31. Nam, S., Lee, J., Brownfield, D. G. & Chaudhuri, O. Viscoplasticity enables mechanical remodeling of matrix by cells. *Biophys. J.* **111**, 2296–2308 (2016).
32. George, P. M. et al. Fabrication and biocompatibility of polypyrrole implants suitable for neural prosthetics. *Biomaterials* **26**, 3511–3519 (2005).
33. George, P. M. et al. Electrical preconditioning of stem cells with a conductive polymer scaffold enhances stroke recovery. *Biomaterials* **142**, 31–40 (2017).
34. George, P. M. et al. Three-dimensional conductive constructs for nerve regeneration. *J. Biomed. Mater. Res. A* **91**, 519–527 (2009).
35. Thalhammer, J. G., Vladimirova, M., Bershadsky, B. & Strichartz, G. R. Neurologic evaluation of the rat during sciatic nerve block with lidocaine. *Anesthesiology* **82**, 1013–1025 (1995).
36. Masters, D. B. et al. Prolonged regional nerve blockade by controlled release of local anesthetic from a biodegradable polymer matrix. *Anesthesiology* **79**, 340–346 (1993).
37. Oh, S. S., Hayes, J. M., Sims-Robinson, C., Sullivan, K. A. & Feldman, E. L. The effects of anesthesia on measures of nerve conduction velocity in male C57Bl6/J mice. *Neurosci. Lett.* **483**, 127–131 (2010).
38. Zotova, E. G. & Arezzo, J. C. Noninvasive evaluation of nerve conduction in small diameter fibers in the rat. *Physiol. J.* **2013**, 1–11 (2013).
39. Mokarram, N. et al. Immunoengineering nerve repair. *Proc. Natl Acad. Sci. USA* **26**, E5077–E5084 (2017).
40. Hort-Legrand, C., Noah, L., Mériguet, E. & Mésangeau, D. Motor and sensory nerve conduction velocities in Yucatan minipigs. *Lab. Anim.* **40**, 53–57 (2006).
41. Amanatullah, D. F. et al. Local estrogen axis in the human bone microenvironment regulates estrogenreceptor-positive breast cancer cells. *Breast Cancer Res.* **19**, 121 (2017).
42. Goldner, J. A modification of the Masson trichrome technique for routine laboratory purposes. *Am. J. Pathol.* **14**, 237–243 (1938).

Acknowledgements

We thank P. Chu for her assistance in this work. We thank K. Xu for assistance with statistical analysis. We thank Agfa for providing PEDOT:PSS Orgacon ICP 1050. Part of this work was performed at the Stanford Nano Shared Facilities, supported by the National Science Foundation under award ECCS-1542152. Y.L. is supported by National Science Scholarship (A*STAR, Singapore). This research was supported in part by the Stanford Bio-X seed funding (Z.B.), Stanford University Dean's Postdoctoral Fellowship (S.S.), National Institutes of Health (NIH) F32HD098808 (S.S.), and NIH K08NS089976 (P.G.) and the Alliance for Regenerative Rehabilitation Research and Training supported by NIH P2C HD086843 (P.G.).

Author contributions

Y.L., J.L., S.S., P.G. and Z.B. designed the project and experiments. Y.L., J.L., J.K., S.C., Y.T., W.X., Y.Z. and V.M. developed the materials and performed device fabrication and characterization. Y.L., S.S. and J.L. performed animal experiments. S.S. and K.M. performed animal behavior tests and tissue processing. Y.L., J.L., S.S., J.B.-H.T., P.G. and Z.B. wrote the manuscript. All authors reviewed and commented on the manuscript.

Competing interests

The authors declare no competing interests.

Additional information

Supplementary information is available for this paper at https://doi.org/10.1038/s41587-020-0495-2.

Correspondence and requests for materials should be addressed to P.M.G. or Z.B.

Reprints and permissions information is available at www.nature.com/reprints.

nature research

Corresponding author(s): Zhenan Bao; Paul M George

Last updated by author(s): Mar 5, 2020

Reporting Summary

Nature Research wishes to improve the reproducibility of the work that we publish. This form provides structure for consistency and transparency in reporting. For further information on Nature Research policies, see Authors & Referees and the Editorial Policy Checklist.

Statistics

For all statistical analyses, confirm that the following items are present in the figure legend, table legend, main text, or Methods section.

n/a	Confirmed	
☐	☒	The exact sample size (*n*) for each experimental group/condition, given as a discrete number and unit of measurement
☐	☒	A statement on whether measurements were taken from distinct samples or whether the same sample was measured repeatedly
☐	☒	The statistical test(s) used AND whether they are one- or two-sided *Only common tests should be described solely by name; describe more complex techniques in the Methods section.*
☒	☐	A description of all covariates tested
☒	☐	A description of any assumptions or corrections, such as tests of normality and adjustment for multiple comparisons
☐	☒	A full description of the statistical parameters including central tendency (e.g. means) or other basic estimates (e.g. regression coefficient) AND variation (e.g. standard deviation) or associated estimates of uncertainty (e.g. confidence intervals)
☐	☒	For null hypothesis testing, the test statistic (e.g. *F*, *t*, *r*) with confidence intervals, effect sizes, degrees of freedom and *P* value noted *Give P values as exact values whenever suitable.*
☒	☐	For Bayesian analysis, information on the choice of priors and Markov chain Monte Carlo settings
☒	☐	For hierarchical and complex designs, identification of the appropriate level for tests and full reporting of outcomes
☒	☐	Estimates of effect sizes (e.g. Cohen's *d*, Pearson's *r*), indicating how they were calculated

Our web collection on statistics for biologists contains articles on many of the points above.

Software and code

Policy information about availability of computer code

Data collection	Electrochemical-impedance and cyclic-voltammetry data were collected with EC-Lab and PSTrace5 and mechanical tests were collected with Bluehill 3 Testing Software. Current-density data were collected by means of the Model 4200-SCS Keithley Test Environment Interactive (KTEI, Tektronix). Rheology data were collected by using TRIOS software (ARES-G2, TA instrument). Evoked compound action potentials were recorded using the Labchart (Powerlab, AD Instrument).
Data analysis	Electrochemical-impedance and cyclic-voltammetry data were analysed by using EC-Lab. Mechanical test data, UV-vis, rehology and current-density and recorded compound action potential data were analysed by using OriginPro 2016 b9.3.226 (64-bit) and Microsoft Excel 2016 (version 1807, 10325.20082). Immunofluorescence data were analysed by using ImageJ (Fiji), OriginPro 2016 b9.3.226 (64-bit) and Microsoft Excel 2016 (version 1807,10325.20082). P value was calculated by software Prism and R. The projection X-ray images were reconstructed into 3D images and processed using software Dragonfly (Object Research System).

For manuscripts utilizing custom algorithms or software that are central to the research but not yet described in published literature, software must be made available to editors/reviewers. We strongly encourage code deposition in a community repository (e.g. GitHub). See the Nature Research guidelines for submitting code & software for further information.

Data

Policy information about availability of data

All manuscripts must include a data availability statement. This statement should provide the following information, where applicable:

- Accession codes, unique identifiers, or web links for publicly available datasets
- A list of figures that have associated raw data
- A description of any restrictions on data availability

The authors declare that all data supporting the findings of this study are available within the paper and its Supplementary Information.

Field-specific reporting

Please select the one below that is the best fit for your research. If you are not sure, read the appropriate sections before making your selection.

☒ Life sciences ☐ Behavioural & social sciences ☐ Ecological, evolutionary & environmental sciences

For a reference copy of the document with all sections, see nature.com/documents/nr-reporting-summary-flat.pdf

Life sciences study design

All studies must disclose on these points even when the disclosure is negative.

Sample size	Sample size was not calculated beforehand. Sample size was determined by the number of biological and technical replicates necessary to convince us that the effect was real. The number of biological replicates we aimed for was at least 3, with several technical replicates in each sample.
Data exclusions	No data were excluded from the analyses.
Replication	All experimental findings, including SEM images, microCT, electrochemical characterization, electrical recording and animal experiments, were reliably reproduced.
Randomization	Experimental groups were formed based on what was being tested with random selections. The same type of animals were used for all experiments.
Blinding	Animals were divided into matched groups and behavior testing was performed by double-blinded individuals.

Reporting for specific materials, systems and methods

We require information from authors about some types of materials, experimental systems and methods used in many studies. Here, indicate whether each material, system or method listed is relevant to your study. If you are not sure if a list item applies to your research, read the appropriate section before selecting a response.

Materials & experimental systems

n/a	Involved in the study
☐	☒ Antibodies
☒	☐ Eukaryotic cell lines
☒	☐ Palaeontology
☐	☒ Animals and other organisms
☒	☐ Human research participants
☒	☐ Clinical data

Methods

n/a	Involved in the study
☒	☐ ChIP-seq
☒	☐ Flow cytometry
☒	☐ MRI-based neuroimaging

Antibodies

Antibodies used	Primary antibodies used in this work include anti-S100 (Abcam ab52642); anti-neurofilament (Abcam ab8135); anti-ED1 (Millipore SigmaMAB1435); Secondary antibodies used in this work include Goat AntiRabbit IgG H&L (Alexa Fluor® 488) (Abcam ab150077), Goat Anti-Mouse IgG H&L (Alexa Fluor® 647) (Abcam ab150115).
Validation	Validation of each antibody was done under standard information offered by the supplier.

Animals and other organisms

Policy information about studies involving animals; ARRIVE guidelines recommended for reporting animal research

Laboratory animals	Male Sprague Dawley rats (Charles River) were used.
Wild animals	The study did not involve wild animals
Field-collected samples	The study did not involve field-collected samples
Ethics oversight	All procedures involving implantation and harvesting of electrodes on rat sciatic nerves were performed in accordance with protocols approved by the Institutional Animal Care and Use Committee (IACUC) at the Stanford University.

Note that full information on the approval of the study protocol must also be provided in the manuscript.